IOP Publishing Classical and Quantum Gravity
Class. Quantum Grav. **37** (2020) 075018 (13pp) https://doi.org/10.1088/1361-6382/ab74f9

Spinning and excited black holes in Einstein-scalar-Gauss–Bonnet theory

Lucas G Collodel[1,2], Burkhard Kleihaus[2], Jutta Kunz[2] and Emanuele Berti[3]

[1] Theoretical Astrophysics, Eberhard Karls University of Tübingen, D-72076 Tübingen, Germany
[2] Institut für Physik, Universität Oldenburg, Postfach 2503, D-26111 Oldenburg, Germany
[3] Department of Physics and Astronomy, Johns Hopkins University, Baltimore, MD 21218, United States of America

E-mail: lucas.gardai-collodel@uni-tuebingen.de

Received 17 December 2019, revised 7 February 2020
Accepted for publication 11 February 2020
Published 5 March 2020

Abstract

We construct rotating black holes in Einstein-scalar-Gauss–Bonnet theory with a quadratic coupling function. We map the domain of existence of the rotating fundamental solutions, we construct radially excited rotating black holes (including their existence lines), and we show that there are angularly excited rotating black holes. The bifurcation points of the radially and angularly excited solutions branching out of the Schwarzschild solution follow a regular pattern.

Keywords: Einstein-scalar–Gauss–Bonnet, roating hairy black holes, excited scalar fields

1. Introduction

In general relativity (GR) the existence of asymptotically flat black holes is subject to severe constraints, often termed no-hair theorems (see e.g. [1–3]). In generalized theories of gravity, on the other hand, less restrictions may arise and thus these may lead to interesting new kinds of asymptotically flat black holes, that carry hair (see e.g. [4]). These hairy black holes might in fact represent contenders to explain current astrophysical observations [5, 6].

A particularly interesting class of generalized theories of gravity is represented by metric theories with higher curvature terms. Such theories arise, for instance, in the low-energy limit of string theory, where these higher curvature terms are accompanied by a scalar field, the dilaton [7, 8]. The resulting black holes then carry scalar hair, as shown for the case of a Gauss–Bonnet (GB) term coupled to a dilaton [9–12].

The physical properties of nonrotating hairy black holes can differ significantly from their GR counterparts, the Schwarzschild black holes. In particular, the presence of the scalar field will give rise to additional branches in the black hole quasinormal mode spectrum [12–15]. When set into rotation, the quadrupole moments of these hairy black holes can exhibit large deviations from those of Kerr black holes, and their angular momentum may even exceed the Kerr bound, $j = J/M^2 = 1$ [16–21]. In constrast, the shadows of hairy black holes and their x-ray reflection spectrum will be very close to those of Kerr black holes [22, 23].

Einstein-dilaton-Gauss–Bonnet gravity is characterized by an exponential coupling function $f(\phi)$ to the GB term, whose exponent is linear in the dilaton field ϕ. Therefore Schwarzschild or Kerr black holes are not solutions of the theory: they are only approached asymptotically. If, however, one allows for other choices of the coupling function (the simplest being a quadratic coupling function $f(\phi) \propto \phi^2$) Schwarzschild and Kerr black holes can be solutions of the theory, and an interesting new phenomenon can arise: curvature-induced spontaneous scalarization of black holes [24–32].

Spontaneous scalarization was first observed in neutron stars within scalar-tensor theory. Here the instability arises when the product $-\beta_0 T$, where β_0 is the effective linear matter-scalar coupling and T is the trace of the stress-energy tensor, is larger than some critical value [33]: spontaneous scalarization is induced by couplings with matter (see also [34, 35], and [42, 43] for matter-induced scalarization in black hole spacetimes). Later it was realized that spontaneous scalarization can occur for charged black holes in Einstein–Maxwell-scalar (EMs) theory, for certain choices of the scalar coupling function and coupling strength [36–41]. This 'charge-induced' spontaneous scalarization presents many similarities with the case of curvature-induced spontaneous scalarization of black holes [24–32].

In Einstein-scalar-Gauss–Bonnet (EsGB) gravity, the presence of black holes with scalar hair that is spontaneously induced by curvature is associated with instabilities of Schwarzschild black holes. In particular, as the coupling constant λ/M is varied, a set of bifurcation points arises, where branches of scalarized black holes emerge [24, 25]. Labelling these bifurcation points by the integer n, the scalarized solutions on the nth branch possess n radial nodes. Thus, besides the fundamental ($n = 0$) scalarized black hole, one can have radially excited modes with $n > 0$. With every new bifurcation point the Schwarzschild black hole gains another unstable mode [28]. The stability of the fundamental static solution depends on the coupling function [24–30, 32] and on self-interaction terms, if they are present [31].

Recently [32], studied the fundamental ($n = 0$) solution for rotating BHs in EsGB theory with a 'Gaussian' coupling function of the form $\mathrm{e}^{-\phi^2}$, as well as its domain of existence and various of its physical properties. The domain of existence is quite broad for small rotation rates (as expected from the static solution), but it becomes narrower as rotation increases. This fact has been exploited in calculations of the shadow of such black holes, which might be used to put a bound on the coupling constant [32].

Here we consider the static and rotating black holes of EsGB theory with a simple quadratic coupling function. We explore the domain of existence of the fundamental rotating black holes and consider their first radial excitations. Moreover, we show that the scalarized static and rotating black holes also possess angular excitations (labelled by an angular integer l). We determine the bifurcation points of the lowest excitations and determine the existence lines of some of the resulting radially and angularly excited rotating black holes. In section 2 we describe the theory and the general properties of axially symmetric EsGB black holes. In section 3 we present our numerical results, and in section 4 we outline possible directions for future work.

2. General framework

2.1. Action

The action of EsGB gravity is

$$S = \frac{1}{16\pi}\int \mathrm{d}^4x\sqrt{-g}\left[R - \frac{1}{2}(\partial_\mu\phi)^2 + f(\phi)R^2_{\rm GB}\right], \tag{1}$$

where ϕ is a (real) scalar field, $f(\phi)$ is the coupling function of the theory, and

$$R^2_{\rm GB} = R_{\mu\nu\rho\sigma}R^{\mu\nu\rho\sigma} - 4R_{\mu\nu}R^{\mu\nu} + R^2 \tag{2}$$

is the Gauss–Bonnet invariant, which would not yield any modifications of the Einstein equations when $f(\phi)$ is a constant, because it corresponds to a boundary term in the action. This is no longer the case if the GB invariant couples to dynamical matter fields. Note that here and below we use geometrical units ($c = G = 1$).

Here we consider the coupling function [25, 28]

$$f(\phi) = \frac{\lambda^2}{8}\phi^2, \tag{3}$$

i.e. a purely quadratic coupling. We will compare our results with those for a Gaussian coupling

$$f(\phi) = \frac{\lambda^2}{12}\left(1 - \mathrm{e}^{-3\phi^2/2}\right), \tag{4}$$

which was studied in [24, 28, 32].

Varying the action (1) with respect to the metric $g_{\mu\nu}$, we obtain the generalized Einstein equations with contributions from the GB term

$$E_{\mu\nu} = G_{\mu\nu} - \frac{1}{2}T^{(\phi)}_{\mu\nu} + f(\phi)H_{\mu\nu} + 4\nabla^\rho\nabla^\sigma f(\phi)P_{\mu\rho\nu\sigma} = 0, \tag{5}$$

where

$$\begin{aligned} G_{\mu\nu} &= R_{\mu\nu} - \frac{1}{2}g_{\mu\nu}R, \quad T^{(\phi)}_{\mu\nu} = \nabla_\mu\phi\nabla_\nu\phi - \frac{1}{2}g_{\mu\nu}(\nabla\phi)^2, \\ H_{\mu\nu} &= 2\big(RR_{\mu\nu} - 2R_{\mu\rho}R^\rho{}_\nu - 2R^{\rho\sigma}R_{\mu\rho\nu\sigma} + R_\mu{}^{\rho\sigma\lambda}R_{\nu\rho\sigma\lambda}\big) - \frac{1}{2}g_{\mu\nu}R^2_{\rm GB}, \\ P_{\mu\nu\rho\sigma} &= R_{\mu\nu\rho\sigma} + 2g_{\mu[\sigma}R_{\rho]\nu} + 2g_{\nu[\rho}R_{\sigma]\mu} + Rg_{\mu[\rho}g_{\sigma]\nu}. \end{aligned} \tag{6}$$

In the above relations, we denote by $P_{\mu\nu\rho\sigma}$ the divergence free part of the Riemann tensor, i.e. $\nabla_\mu P^\mu{}_{\nu\rho\sigma} = 0$. Obviously, the equations (5) can be written in an Einstein-like form

$$G_{\mu\nu} = \frac{1}{2}T^{(\rm eff)}_{\mu\nu}, \tag{7}$$

where we have introduced an effective energy-momentum tensor that has acquired a contribution arising from the GB term

$$T^{(\rm eff)}_{\mu\nu} = T^{(\phi)}_{\mu\nu} - 2T^{(\rm GB)}_{\mu\nu}, \tag{8}$$

with

$$T^{(\rm GB)}_{\mu\nu} = f(\phi)H_{\mu\nu} + 4\nabla^\rho\nabla^\sigma f(\phi)P_{\mu\rho\nu\sigma}. \tag{9}$$

Variation of equation (1) with respect to the scalar field leads to a generalized Klein–Gordon equation,

$$\nabla^2\phi + \frac{\mathrm{d}f}{\mathrm{d}\phi}R^2_{\mathrm{GB}} = 0. \tag{10}$$

2.2. The ansatz and equations of motion

We would like to focus on stationary, axially symmetric spacetimes possessing two commuting Killing vector fields, ξ and η, with

$$\xi = \partial_t \ \text{ and } \ \eta = \partial_\varphi \tag{11}$$

in a system of adapted coordinates. Such spacetimes are typically described by a Lewis–Papapetrou–type ansatz [44], which satisfies the circularity condition and contains four unknown functions. Here we employ the version of this ansatz originally introduced in [45], with the parametrization

$$\mathrm{d}s^2 = -b\mathrm{e}^{F_0}\mathrm{d}t^2 + \mathrm{e}^{F_1}\left(\mathrm{d}r^2 + r^2\mathrm{d}\theta^2\right) + \mathrm{e}^{F_2}r^2\sin^2\theta(\mathrm{d}\varphi - \frac{\omega}{r}\mathrm{d}t)^2, \tag{12}$$

where r, θ, and φ are 'quasi-isotropic' spherical coordinates, and t is the time coordinate. Here $b = (1 - \frac{r}{r_{\mathrm{H}}})^2$ is an auxiliary function, and r_{H} denotes the isotropic horizon coordinate. The metric functions F_0, F_1, F_2 and ω depend on the coordinates r and θ. The scalar field is also a function of r and θ only:

$$\phi = \phi(r, \theta). \tag{13}$$

2.3. Boundary conditions and asymptotic behavior

2.3.1. Large-r asymptotics. We here consider solutions that approach a Minkowski spacetime background as $r \to \infty$. This implies the following boundary conditions:

$$F_0(\infty) = F_1(\infty) = F_2(\infty) = \omega(\infty) = \phi(\infty) = 0\,. \tag{14}$$

Since the scalar field is massless, one can construct an approximate solution of the field equations (5) and (10), that is compatible with these asymptotic conditions as a power series in $1/r$.

2.3.2. Expansion on the event horizon. The event horizon of the (non-extremal) stationary black hole solutions resides at a surface of constant radial coordinate, $r = r_{\mathrm{H}} > 0$. Again, it is possible to construct an approximate (power series) solution, this time in terms of

$$\delta = \frac{r}{r_{\mathrm{H}}} - 1. \tag{15}$$

Demanding that the metric functions and the scalar field, as well as their derivatives are not diverging at the horizon leads to the conditions

$$\partial_r F_0(r_{\mathrm{H}}) = \frac{1}{r_{\mathrm{H}}}, \quad \partial_r F_1(r_{\mathrm{H}}) = -\frac{2}{r_{\mathrm{H}}}, \quad \partial_r F_2(r_{\mathrm{H}}) = -\frac{2}{r_{\mathrm{H}}}, \quad \omega(r_{\mathrm{H}}) = \omega_{\mathrm{H}}, \quad \partial_r\phi(r_{\mathrm{H}}) = 0, \tag{16}$$

where ω_{H} is a constant. Note that, similar to the case of pure Einstein gravity, the equation $E^\theta_r = 0$ implies that the ratio F_0/F_1 is constant at the horizon. This implies the constancy

of the Hawking temperature, and also represents a supplementary condition which is used as further test of numerical accuracy.

2.3.3. Behavior on the symmetry axis. Axial symmetry and regularity impose the following boundary conditions for the metric functions on the symmetry axis (i.e. at $\theta = 0, \pi$):

$$\partial_\theta F_0|_{\theta=0,\pi} = \partial_\theta F_1|_{\theta=0,\pi} = \partial_\theta F_2|_{\theta=0,\pi} = \partial_\theta \omega|_{\theta=0,\pi} = 0, \tag{17}$$

while for the scalar field we impose

$$\partial_\theta \phi|_{\theta=0,\pi} = 0. \tag{18}$$

Near the symmetry axis it is possible to construct an approximate form of the solutions as a power series, now in terms of θ (and $\pi - \theta$, respectively). Further, the absence of conical singularities implies $F_1|_{\theta=0,\pi} = F_2|_{\theta=0,\pi}$.

All fundamental solutions discussed here are symmetric with respect to reflection across the equatorial plane, $\theta = \pi/2$. Therefore, in the numerical calculations, it is sufficient to consider the range $0 \leqslant \theta \leqslant \pi/2$ for the angular variable θ. Then the metric functions and the scalar field are required to satisfy Neumann boundary conditions in the equatorial plane:

$$\partial_\theta F_0|_{\theta=\pi/2} = \partial_\theta F_1|_{\theta=\pi/2} = \partial_\theta F_2|_{\theta=\pi/2} = \partial_\theta \omega|_{\theta=\pi/2} = \partial_\theta \phi|_{\theta=\pi/2} = 0. \tag{19}$$

Note that the scalar field of the first angular excitation possesses odd parity. In this case the boundary condition in the equatorial plane reads $\phi|_{\theta=\pi/2} = 0$.

2.4. Physical properties

Let us now briefly address the physical properties of these black holes. Starting with the horizon properties, we note that the metric of a spatial cross section of the horizon is

$$d\Sigma^2 = h_{ij} \mathrm{d}x^i \mathrm{d}x^j = r_{\mathrm{H}}^2 \left(\mathrm{e}^{F_1} \mathrm{d}\theta^2 + \mathrm{e}^{F_2} \sin^2\theta \mathrm{d}\varphi^2 \right)\big|_{r_{\mathrm{H}}}. \tag{20}$$

The Killing vector field

$$\chi = \partial_t - \frac{\omega_{\mathrm{H}}}{r_{\mathrm{H}}} \partial_\varphi \tag{21}$$

is orthogonal to (and null on) the horizon [44]. The boundary parameter ω_{H} defined in equation (16) determines the horizon angular velocity Ω_{H}

$$\Omega_{\mathrm{H}} = -\frac{\xi^2}{\xi \cdot \eta} = -\left. \frac{g_{\varphi t}}{g_{tt}} \right|_{r_{\mathrm{H}}} = \frac{\omega_{\mathrm{H}}}{r_{\mathrm{H}}}. \tag{22}$$

The Hawking temperature $T_{\mathrm{H}} = \kappa/(2\pi)$ is obtained from the surface gravity κ [44], where $\kappa^2 = -\frac{1}{2}(\nabla_a \chi_b)(\nabla^a \chi^b)|_{r_{\mathrm{H}}}$, yielding

$$T_{\mathrm{H}} = \frac{1}{2\pi r_{\mathrm{H}}} \mathrm{e}^{(F_0 - F_1)/2}. \tag{23}$$

The horizon area of the black holes is given by

$$A_{\mathrm{H}} = 2\pi r_{\mathrm{H}}^2 \int_0^\pi \mathrm{d}\theta \sin\theta \mathrm{e}^{(F_0 + F_2)/2}. \tag{24}$$

Black holes in GR possess an entropy which is a quarter of the horizon area [44]. However, because of the scalar coupling to the GB term, the entropy of the EsGB black holes acquires

an extra contribution. Following Wald [47], the total entropy can then be given as an integral over the horizon

$$S = \frac{1}{4}\int_{\Sigma_{\rm H}} \mathrm{d}^2x\sqrt{h}(1+2f(\phi)\tilde{R}), \tag{25}$$

where h is the determinant of the induced metric on the horizon (defined in (20)), and $\tilde{R}$ is defined as the scalar curvature of the induced metric on a slice of constant time of the horizon. Explicitly, we have

$$\tilde{R} = -\frac{\mathrm{e}^{-F_1}}{2r_{\rm H}^2\sin\theta}\left(\left[2(\partial_\theta^2 F_2 - 2) + (\partial_\theta F_2)^2 - \partial_\theta F_1\partial_\theta F_2\right]\sin\theta - 2\left[\partial_\theta F_1 - 2\partial_\theta F_2\right]\cos\theta\right), \tag{26}$$

where all functions are evaluated at $r = r_{\rm H}$.

Similar to GR solutions, the total mass M and the angular momentum J are read from the asymptotic behavior of the metric functions

$$\begin{aligned} g_{tt} &= -\mathrm{e}^{F_0} + \mathrm{e}^{F_2}\omega^2\sin^2\theta = -1 + \frac{2M}{r} + \ldots, \\ g_{\varphi t} &= -\mathrm{e}^{F_2}\omega^2\sin^2\theta = -\frac{2J}{r}\sin^2\theta + \ldots. \end{aligned} \tag{27}$$

In addition, the solutions possess a scalar 'charge' D, which is determined by the $1/r$ term of the far-field asymptotics of the scalar field.

2.5. Numerical approach

Let us briefly address the numerical approach employed to construct the EsGB black holes. The unknown metric and scalar field functions $(F_0, F_1, F_2, \omega; \phi)$ are obtained as solutions of a rather lengthy coupled set of partial differential equations (PDEs), subject to the associated set of boundary conditions, guaranteeing regularity and asymptotic flatness.

The only non-trivial components of the generalized Einstein equations (5) are $E^t_t, E^r_r, E^\theta_\theta, E^\varphi_\varphi, E^t_\varphi$ and E^θ_r. Following [45], we divide the resulting six equations into two groups. Four equations for the metric functions are obtained from a suitable linear combination of $E^t_t, E^\varphi_\varphi, E^t_\varphi$ and $E^r_r + E^\theta_\theta$. The remaining two equations ($E^r_r - E^\theta_\theta$ and E^θ_r) represent constraints. We solve the four equations together with the scalar field equation (10), each containing more than 340 independent terms, while we follow the two constraints to check the accuracy of the numerical solutions.

The domain of integration corresponds to the region outside the horizon. We therefore introduce a new radial variable $x = 1 - r_{\rm H}/r$, which maps the semi-infinite interval $[r_{\rm H}, \infty)$ to the closed interval $[0, 1]$. We then discretize the equations on a non-equidistant grid in x and θ. Typical grids used have sizes 91×51, and cover the integration region $0 \leqslant x \leqslant 1$ and $0 \leqslant \theta \leqslant \pi/2$. We perform the numerical calculations using the professional package FIDISOL/CADSOL [46], which is based on a Newton–Raphson method. The typical numerical error for the functions is estimated to be lower than 10^{-3}.

For each solution we provide three input parameters, λ, $r_{\rm H}$ and $\Omega_{\rm H} = \frac{\omega_{\rm H}}{r_{\rm H}}$. After convergence has been reached, the physical properties are computed from the numerical solutions. In particular, the mass M and the angular momentum J are obtained from the asymptotic behavior of the solutions (27), whereas the horizon area $A_{\rm H}$, the entropy S and the temperature $T_{\rm H}$ are extracted from the horizon metric.

3. Results

Before we turn to rotating black holes, let us briefly recall the properties of static black holes in this theory [25, 28]. The bifurcation points of the sets of static scalarized black holes from the branch of Schwarzschild black holes have been obtained for the quadratic coupling function in [25], and they agree with those of the exponential coupling [24], since the latter reduces to the quadratic coupling in the limit of small scalar field. The fundamental ($n = 0$) static branch thus arises at the bifurcation point $M/\lambda = 0.587$, where the Schwarzschild solution developes a zero mode, which turns into a first unstable radial mode for smaller M/λ. At the nth ($n > 0$) bifurcation point, the Schwarzschild solution developes the $(n + 1)$th unstable radial mode, while the associated nth branch of scalarized black hole solutions possesses n radial nodes and $(n + 1)$ unstable radial modes. Thus all scalarized black hole solutions are unstable, including the fundamental solution [28]. Furthermore we note that all branches of static scalarized black hole solutions exist only in a small domain that decreases with increasing n, as illustrated by the solid blue curves in figure 1(a), where their scaled scalar charge Q/M is shown versus the scaled mass M/λ. Note, that the figure also contains some angularly excited solutions (dashed red: $l = 1$, green dots: $l = 2$) discussed below.

In the following we present our results, starting with the domain of existence of the fundamental rotating solutions. Subsequently, we address rotating radial excitations and angular excitations.

3.1. Fundamental rotating black holes

The fundamental static black holes exist only in a small interval of M/λ. As these black holes are set into rotation, this small interval shrinks further, as seen in figure 1(b) where we plot the scaled angular momentum J/λ^2 as a function of the scaled mass M/λ. The boundaries of the domain of existence correspond to the 'existence line' to the left (solid blue line starting at $M/\lambda = 0.587$), and the critical (dashed blue) line on the right where hairy solutions cease to exist: beyond the critical line, there are only complex solutions for the scalar field.

The domain of existence resides fully within the domain of existence of the Kerr black holes for the angular momenta studied. As the scaled angular momentum J/λ^2 increases, the domain of existence of the scalarized black holes tends towards the set of extremal Kerr black holes. We note that this behavior is rather similar to the case of exponential coupling [32]. However, in the latter case, the domain of static scalarized black holes extends from the existence point all the way to $M/\lambda = 0$, yielding a large domain of existence for small angular momenta J/λ^2.

In figure 2(a) we illustrate the domain of existence by plotting the scaled scalar charge Q/M as a function of the scaled angular momentum $j = J/M^2$. The scalar charge decreases with the angular momentum, i.e. it decreases as we approach the extremal Kerr limit, where $Q/M = 0$. On the other hand, figure 2(b) shows the domain of existence with respect to the coupling constant. It also includes curves of constant $\omega_{\rm H}$, which for constant $r_{\rm H}$ corresponds to a constant angular velocity of the horizon $\Omega_{\rm H}$ (see equation (22)). Interestingly, the static curve does not describe the boundary curve here, but λ/M can slightly exceed this curve for small rotation.

As demonstrated in figure 3(a), the scaled horizon mass $M_{\rm H}/M$ is typically slightly smaller than one. Again, for large angular momenta this is similar to the exponential coupling case, where, however, much larger deviations are observed for small angular momenta [32]. Figure 3(b) exhibits the domain of existence for the scaled area $A_{\rm H}/16\pi M^2$.

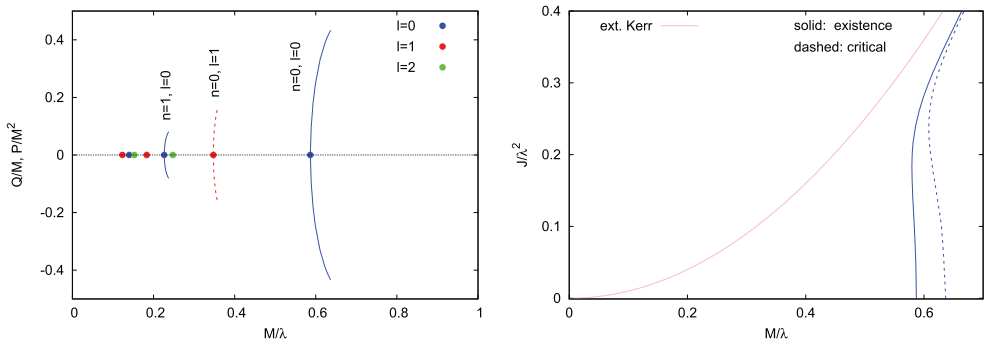

Figure 1. Domain of existence of scalarized black holes: (a) fundamental and radially and angularly excited static solutions: scaled scalar charge Q/M versus scaled mass M/λ for even l ($l = 0$: solid blue, $l = 2$: green), scaled dipole moment P/M^2 versus scaled mass M/λ ($l = 1$: dashed red); (b) fundamental rotating solutions: scaled angular momentum J/λ^2 versus scaled mass M/λ (existence line: solid blue, critical line: dashed blue). Also shown are the extremal Kerr solutions (solid red).

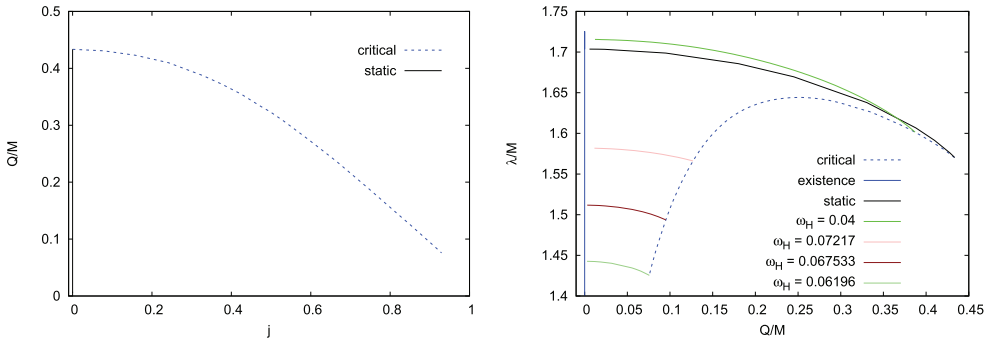

Figure 2. Domain of existence of fundamental rotating scalarized black holes: (a) scaled scalar charge Q/M versus scaled angular momentum $j = J/M^2$ (critical line: dashed blue, static solutions: solid black); (b) scaled coupling constant λ/M versus scaled scalar charge Q/M (existence line: solid blue, critical line: dashed blue, static solutions: solid black), for several fixed values of the horizon parameter $\omega_{\rm H} = \Omega_{\rm H} r_{\rm H}$.

The horizon area is smaller than in the Kerr case, but nowhere are the deviations between the two very large. As noted in [32], large deviations are possible for Gaussian coupling functions, and this can be used to put bounds on the coupling via the black hole shadow of M87 [48].

Of considerable interest for such scalarized black holes is the calculation of the entropy, which differs from the corresponding value obtained from the horizon area. If the entropy for the scalarized solutions is larger than the entropy for Kerr (or Schwarzschild) black holes, this is an indication that the scalarized solutions will be stable. Here we do not expect stability, since static black holes are already known to be unstable. Indeed, figure 3(b) shows an explicit calculation of the scaled entropy, which is smaller than in GR (as expected). However, the domain of existence for the entropy of the scalarized solutions is extremely close to the case of Kerr black holes. The difference is highlighted in the lower inset of figure 3(b).

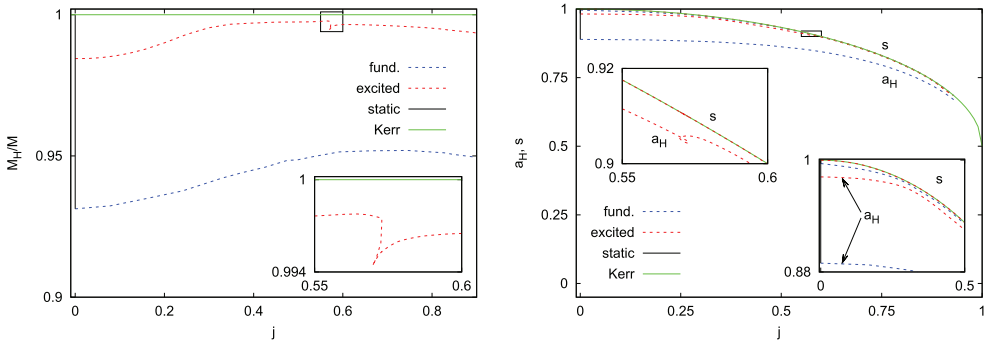

Figure 3. Domain of existence of fundamental and first radially excited rotating scalarized black holes: (a) scaled horizon mass $M_{\rm H}/M$ versus scaled angular momentum j (critical line: dashed blue (fundamental), dashed red (first radially excited), static line: solid black, Kerr solutions: green); (b) scaled horizon area $a_{\rm H} = A_{\rm H}/16\pi M^2$ and scaled entropy $s = S/4\pi M^2$ versus scaled angular momentum j, (same linestyles as in (a)). The lower inset illustrates the small difference in entropy.

3.2. Excited static black holes

Scalarized black holes come in many variants. Besides the well-studied radial excitations, labeled by the integer n, there are also angular excitations and combinations of both. In the static limit, this is easily seen when expanding the scalar field in terms of spherical harmonics

$$\phi = \sum_{lm} f_l(r) Y_{lm}(\theta, \varphi) \tag{28}$$

involving the integers l and m. We exhibit the bifurcation points of the lowest radially and angularly excited static scalarized black holes in figure 4, where the scaled coupling constant λ/M is shown versus angular excitations, labelled by the integer l, for the lowest radial excitations (labelled by the integer n). Interestingly, the observed pattern of bifurcation points is highly regular, formed by adjacent rhomboids (see also [51]).

Let us now consider the extension of the associated radially and angularly excited static solutions, restricting attention to their existence lines, where the scalar field equation is solved in the background of the Schwarzschild black hole. For these existence lines, figure 5(a) shows the scaled scalar charge Q/M (solid lines) and the scaled dipole moment P/M^2 (dashed lines) as functions of the scaled mass M/λ. In particular, we show solutions with $n = 0, l = 0$ (fundamental), $n = 0, l = 1$ (one angular excitation) $n = 0, l = 2$ (two angular excitations) and $n = 1, l = 0$ (one radial excitation). The dots in the figure indicate the bifurcation points from the Schwarzschild black holes for $l = 0$ (blue), $l = 1$ (red) and $l = 2$ (green). Note that solutions with $l = 1$ possess a parity-odd scalar field, therefore they do not carry scalar charge. The dipole term represents the lowest term in their asymptotic expansion, so in the figure we plot their dipole moment.

We can ask whether static excited black holes are stable. A glance at their entropy—as shown in figure 5(b)—indicates that not only the radially excited static solutions are unstable [28], but also the angularly excited solutions should be unstable.

Of course, one might also consider static solutions, that in the presence of backreaction will lose axial symmetry. Examples would be black holes labelled by the above set of 3 integers (n, l, m), where the azimuthal integer $m \neq 0$, as in the solutions considered in [38]. For given integers n and l, these would possess a degenerate bifurcation point for all allowed values of

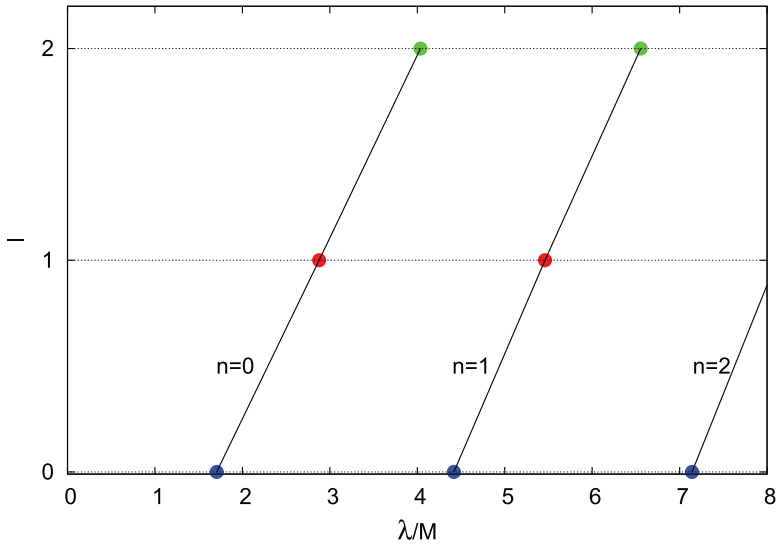

Figure 4. Bifurcation points of excited static scalarized black holes: scaled coupling constant λ/M versus angular integer l for the lowest radial excitations n; $l = 0$ (blue), $l = 1$ (red) and $l = 2$ (green).

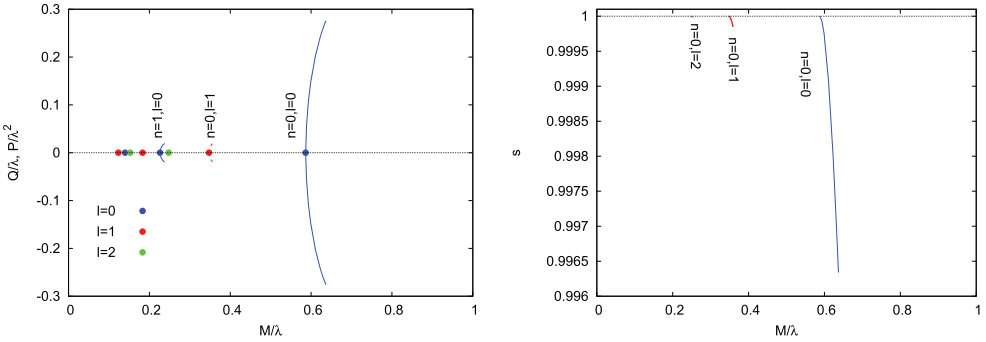

Figure 5. Excited static scalarized black holes: (a) scaled scalar charge Q/λ for even l ($l = 0$: solid blue, $l = 2$: green), and scaled dipole moment P/λ^2 ($l = 1$: dashed red) versus scaled mass M/λ; (b) scaled entropy $s = S/4\pi M^2$ versus scaled mass M/λ for the lowest radial and angular exitations. Bifurcation points: $l = 0$ (blue), $l = 1$ (red) and $l = 2$ (green).

m, but give rise to a set of $l + 1$ distinct families of scalarized black holes, one with axial symmetry ($m = 0$) and l without any continuous symmetry ($m \neq 1$).

3.3. Excited rotating black holes

Let us next consider excited rotating scalarized black holes. We show the existence line for several such black holes in figure 6(a). In particular, in addition to the fundamental solution for $l = 0$, $n = 0$ (blue), the figure exhibits the existence line for its first radial excitation $l = 0$, $n = 1$ (blue), together with the existence line of two branches of solutions starting from the bifurcation points $l = 2$, $n = 0$ and $l = 2$, $n = 1$ (green). As seen in the figure, the existence

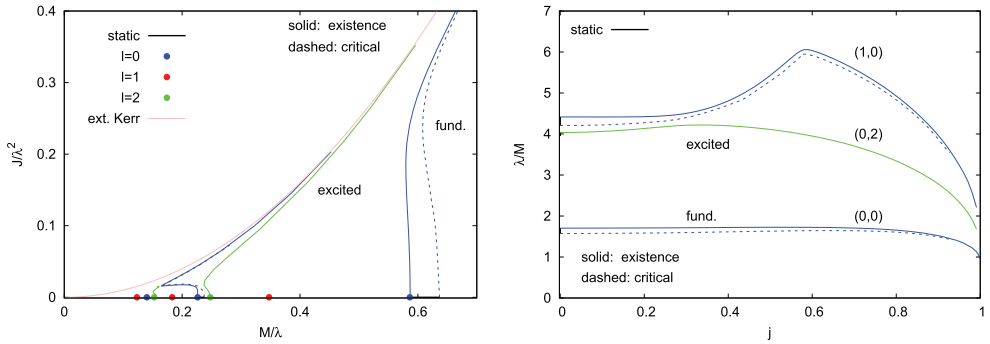

Figure 6. Excited rotating scalarized black holes: (a) scaled angular momentum J/λ^2 versus scaled mass M/λ; (b) scaled coupling constant λ/M versus scaled angular momentum j. Shown are $(n,l)=(0,0)$ (blue), $(n,l)=(1,0)$ (blue), $(n,l)=(0,2)$ (green) (existence lines: solid, critical lines: dashed).

lines $l=2$, $n=0$ and $l=0$, $n=1$ approach the set of extremal Kerr solutions quite rapidly. Also shown are the critical solutions with $l=0, n=0$ and $l=0, n=1$ (dashed).

In figure 6(b) we plot the existence lines as functions of the scaled coupling constant λ/M and of the scaled angular momentum j. Besides the fundamental rotating solution $(n,l)=(0,0)$, we show also the first radially excited solution $(n,l)=(1,0)$, and the second angularly excited solution $(n,l)=(0,2)$[4]. The short black lines on the axis indicate the domain of existence of the static $(0,0)$ and $(1,0)$ solutions. We have also obtained part of the existence lines of further excited solutions like the second angularly excited solution $(n,l)=(0,2)$; however, these remain challenging to fully map out.

4. Conclusions

Spontaneously scalarized black holes can exist when the coupling function and coupling constant satisfy certain conditions. In this paper we have studied curvature-induced scalarization mediated by the presence of a GB term. In particular, we have focused on a quadratic coupling function, extending previous studies of the fundamental ($n=0$) nonrotating static solution and of its radial excitations.

We have mapped out the domain of existence of rotating generalizations of these solutions, showing that the domain of existence is a small band starting from the static solutions and extending to larger angular momenta. This band shrinks as the angular momentum grows, approaching the extremal Kerr solutions. As for static black holes, the entropy of these rotating scalarized black holes is smaller than the entropy of Kerr black holes, suggesting that rotating scalarized black holes should also be unstable.

We have further considered excited (static and rotating) solutions considering also angular excitations with $l>0$. The bifurcation points form a simple regular pattern in (n,l), at least for small values of n and l. Branches of excited black holes emerge from these bifurcation points: this behavior is similar to the case of static, charge-induced spontaneously scalarized

[4] The first radially excited branches of solutions have also been included in figure 3, where their scaled horizon mass, horizon area and entropy are shown.

black holes [38]. Taking this similarity further, we conjecture that there should also exist static EsGB black holes without any continuous symmetry.

As long as axial symmetry is retained, the excited solutions can also be set into rotation, forming stationary sets of solutions. Here we have mainly explored the existence lines of these radially and angularly excited rotating black holes, but we also constructed solutions with backreaction.

While we do not expect stable spontaneously scalarized black holes for this theory, it should be possible to restore stability by adding higher-order terms to the coupling function [24, 28] or by including a potential term $V(\phi)$ for the scalar field [31, 49]. The latter approach is particularly attractive, since these corrections would emerge naturally in an effective field theory scenario.

Acknowledgments

The authors gratefully acknowledge support by the DFG Research Training Group 1620 *Models of Gravity* and the COST Actions CA15117 *CANTATA* and CA16104 *GWverse*. LC is thankful for the financial support obtained through the DFG Emmy Noether Research Group under Grant No. DO 1771/1-1. EB is supported by NSF Grants No. PHY-1912550 and AST-1841358, NASA ATP Grants No. 17-ATP17-0225 and 19-ATP19-0051, and NSF-XSEDE Grant No. PHY-090003. This work has received funding from the European Union's Horizon 2020 research and innovation programme under the Marie Sklodowska-Curie Grant agreement No. 690904. This research project was conducted using computational resources at the Maryland Advanced Research Computing Center (MARCC). The authors are grateful to Eugen Radu for all the fruitful discussions.

ORCID iDs

Lucas Gardai Collodel https://orcid.org/0000-0002-8162-4450
Burkhard Kleihaus https://orcid.org/0000-0001-9751-4400
Jutta Kunz https://orcid.org/0000-0001-7990-8713
Emanuele Berti https://orcid.org/0000-0003-0751-5130

References

[1] Chrusciel P T, Lopes Costa J and Heusler M 2012 *Living Rev. Relativ.* **15** 7
[2] Herdeiro C A R and Radu E 2015 *Int. J. Mod. Phys.* D **24** 1542014
[3] Cardoso V and Gualtieri L 2016 *Class. Quantum Grav.* **33** 174001
[4] Berti E *et al* 2015 *Class. Quantum Grav.* **32** 243001
[5] Berti E, Yagi K and Yunes N 2018 *Gen. Relativ. Gravit.* **50** 46
[6] Berti E, Yagi K, Yang H and Yunes N 2018 *Gen. Relativ. Gravit.* **50** 49
[7] Gross D J and Sloan J H 1987 *Nucl. Phys.* B **291** 41
[8] Metsaev R R and Tseytlin A A 1987 *Nucl. Phys.* B **293** 385
[9] Kanti P, Mavromatos N E, Rizos J, Tamvakis K and Winstanley E 1996 *Phys. Rev.* D **54** 5049
[10] Torii T, Yajima H and Maeda K I 1997 *Phys. Rev.* D **55** 739
[11] Guo Z K, Ohta N and Torii T 2008 *Prog. Theor. Phys.* **120** 581
[12] Pani P and Cardoso V 2009 *Phys. Rev.* D **79** 084031
[13] Ayzenberg D, Yagi K and Yunes N 2014 *Phys. Rev.* D **89** 044023
[14] Blázquez-Salcedo J L, Macedo C F B, Cardoso V, Ferrari V, Gualtieri L, Khoo F S, Kunz J and Pani P 2016 *Phys. Rev.* D **94** 104024

[15] Blázquez-Salcedo J L, Khoo F S and Kunz J 2017 *Phys. Rev.* D **96** 064008
[16] Pani P, Macedo C F B, Crispino L C B and Cardoso V 2011 *Phys. Rev.* D **84** 087501
[17] Ayzenberg D and Yunes N 2014 *Phys. Rev.* D **90** 044066
[18] Maselli A, Pani P, Gualtieri L and Ferrari V 2015 *Phys. Rev.* D **92** 083014
[19] Kleihaus B, Kunz J and Radu E 2011 *Phys. Rev. Lett.* **106** 151104
[20] Kleihaus B, Kunz J and Mojica S 2014 *Phys. Rev.* D **90** 061501
[21] Kleihaus B, Kunz J, Mojica S and Radu E 2016 *Phys. Rev.* D **93** 044047
[22] Cunha P V P, Herdeiro C A R, Kleihaus B, Kunz J and Radu E 2017 *Phys. Lett.* B **768** 373
[23] Zhang H, Zhou M, Bambi C, Kleihaus B, Kunz J and Radu E 2017 *Phys. Rev.* D **95** 104043
[24] Doneva D D and Yazadjiev S S 2018 *Phys. Rev. Lett.* **120** 131103
[25] Silva H O, Sakstein J, Gualtieri L, Sotiriou T P and Berti E 2018 *Phys. Rev. Lett.* **120** 131104
[26] Antoniou G, Bakopoulos A and Kanti P 2018 *Phys. Rev. Lett.* **120** 131102
[27] Antoniou G, Bakopoulos A and Kanti P 2018 *Phys. Rev.* D **97** 084037
[28] Blázquez-Salcedo J L, Doneva D D, Kunz J and Yazadjiev S S 2018 *Phys. Rev.* D **98** 084011
[29] Doneva D D, Kiorpelidi S, Nedkova P G, Papantonopoulos E and Yazadjiev S S 2018 *Phys. Rev.* D **98** 104056
[30] Silva H O, Macedo C F B, Sotiriou T P, Gualtieri L, Sakstein J and Berti E 2019 *Phys. Rev.* D **99** 064011
[31] Macedo C F B, Sakstein J, Berti E, Gualtieri L, Silva H O and Sotiriou T P 2019 *Phys. Rev.* D **99** 104041
[32] Cunha P V P, Herdeiro C A R and Radu E 2019 *Phys. Rev. Lett.* **123** 011101
[33] Damour T and Esposito-Farese G 1993 *Phys. Rev. Lett.* **70** 2220
[34] Mendes R F P and Ortiz N 2016 *Phys. Rev.* D **93** 124035
[35] Altaha Motahar Z, Blázquez-Salcedo J L, Kleihaus B and Kunz J 2017 *Phys. Rev.* D **96** 064046
[36] Stefanov I Z, Yazadjiev S S and Todorov M D 2008 *Mod. Phys. Lett.* A **23** 2915
[37] Doneva D D, Yazadjiev S S, Kokkotas K D and Stefanov I Z 2010 *Phys. Rev.* D **82** 064030
[38] Herdeiro C A R, Radu E, Sanchis-Gual N and Font J A 2018 *Phys. Rev. Lett.* **121** 101102
[39] Myung Y S and Zou D C 2019 *Eur. Phys. J.* C **79** 273
[40] Myung Y S and Zou D C 2019 *Phys. Lett.* B **790** 400
[41] Myung Y S and Zou D C 2019 *Eur. Phys. J.* C **79** 641
[42] Cardoso V, Carucci I P, Pani P and Sotiriou T P 2013 *Phys. Rev. Lett.* **111** 111101
[43] Cardoso V, Carucci I P, Pani P and Sotiriou T P 2013 *Phys. Rev.* D **88** 044056
[44] Wald R M 1984 *General Relativity* (Chicago, IL: University of Chicago Press) (https://doi.org/10.7208/chicago/9780226870373.001.0001)
[45] Kleihaus B and Kunz J 2001 *Phys. Rev. Lett.* **86** 3704
[46] Schönauer W and Weiß R 1989 *J. Comput. Appl. Math.* **27** 279
Schauder M, Weiß R and Schönauer W 1992 *The CADSOL Program Package* Universität Karlsruhe, Interner Bericht Nr. 46/92
[47] Wald R M 1993 *Phys. Rev.* D **48** R3427
[48] Akiyama K *et al* (Event Horizon Telescope Collaboration) 2019 *Astrophys. J.* **875** L6
[49] Doneva D D, Staykov K V and Yazadjiev S S 2019 *Phys. Rev.* D **99** 104045
[50] Ascher U, Christiansen J and Russell R D 1979 *Math. Comput.* **33** 659
[51] Hod S 2019 *Phys. Rev.* D **100** 064039